Magnetically induced instabilities in duct flows

IOP Conf. Series: Materials Science and Engineering **228** (2017) 012003 doi:10.1088/1757-899X/228/1/012003

Magnetically induced instabilities in duct flows

L Bühler[1], T Arlt[1], T Boeck[2], L Braiden[3], V Chowdhury[1], D Krasnov[2], C Mistrangelo[1], S Molokov[3], J Priede[3]

[1]Karlsruhe Institute of Technology, Postfach 3640, 76021 Karlsruhe
[2] Technische Universität Ilmenau, Postfach 100565, 98684 Ilmenau, Germany
[3]Applied Mathematics Research Centre, Coventry University, Coventry CV1 5FB, UK

leo.buehler@kit.edu

Abstract. The occurrence of magnetically induced instability in magnetohydrodynamic duct flows is studied for Hunt flow, where one pair of walls parallel to the magnetic field is electrically insulating and the Hartmann walls perpendicular to the field are electrically conducting. The onset of time-dependent flow patterns and their intensity depends on the strength of the magnetic field and on the flow rate in terms of the Hartmann and Reynolds numbers, respectively. The problem is studied by a complementary approach using laboratory experiments, linear stability analysis and high-resolution direct numerical simulations.

1. Introduction

Liquid metal flows in channels with arbitrary wall electric conductivity are of importance for engineering applications such as liquid metal blankets for nuclear fusion reactors with magnetic confinement of the plasma. Under the action of strong magnetic fields, liquid metal flows in electrically conducting ducts exhibit jet-like velocity profiles in the thin boundary layers along walls parallel to the magnetic field. The velocity in these so-called side layers may exceed several times the mean velocity in the channel core, depending on magnetic field strength and electrical conductance of the walls. This kind of MHD flow received attention in recent years for validation of numerical tools [1] and it is of fundamental interest since the jet-like velocity distributions are potentially unstable. It is known that the flow in these layers becomes unstable already at relatively small Reynolds numbers [2]. A linear stability analysis [2] predicts a critical Reynolds number for the onset of instabilities, which is almost one order of magnitude smaller than the one obtained experimentally [3] [4]. The discrepancy between theory and experiments was attributed in the latter references by the need of a non-linear stability analysis, or by the influence on the experimental data of 3D effects at the entrance of the magnet. However, a conclusive explanation has not been found yet.

Numerical and experimental investigations of instabilities in parallel boundary layers have received increasing attention in the last years due to their significant influence on heat and mass transfer in liquid metal duct flows and therefore on the performance of liquid metal devices and blankets for fusion reactors. It has been shown that an applied magnetic field tends to damp three-dimensional flow perturbations and supports the formation of two dimensional structures aligned with the magnetic field. The electromagnetic damping of instabilities is exploited e.g. by electromagnetic brakes in metallurgical casting processes.

The present work focuses on the study of the onset of time-dependent instabilities in liquid metal magnetohydrodynamic (MHD) duct flows and the transition of unstable flow patterns to fully developed

MHD turbulence. MHD flows in ducts with electrically conducting Hartmann walls and insulating side walls exhibit highest velocities in side layer jets (strong destabilisation) while Joule dissipation due to the conducting Hartmann walls (damping) should stabilise the flow. From this point of view this so-called Hunt flow [5] constitutes an ideal prototype of magnetically induced instabilities for fundamental research of the influence of these counteracting mechanisms. A sketch of fully established MHD flows in conducting rectangular ducts is shown in Figure 1.

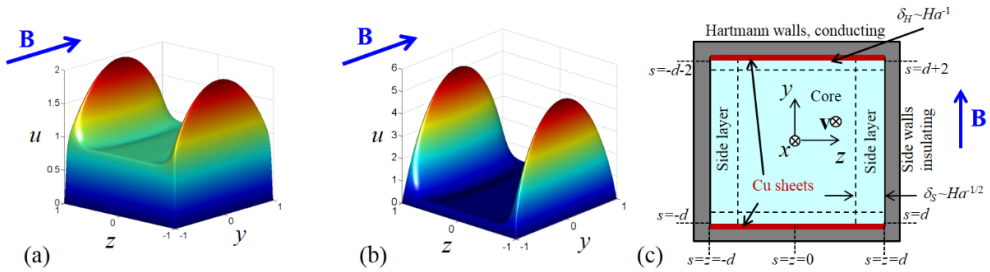

Figure 1. Fully developed velocity profiles in rectangular ducts with all walls conducting (a) and conducting Hartmann walls and insulating side walls (b), sketch of geometry and coordinates used for Hunt flow (c).

2. Problem description

We consider the stability of fully developed laminar duct flow of an electrically conducting incompressible viscous fluid under the influence of a uniform constant magnetic field. The flow is characterized by three non-dimensional groups, Hartmann number, Reynolds number, and wall conductance ratio,

$$Ha = LB\sqrt{\frac{\sigma}{\rho\nu}}, \quad Re = \frac{u_0 L}{\nu}, \quad \text{and } c = \frac{\sigma_w t_w}{\sigma L},$$

where L is a typical length scale of the problem, B the magnitude of the applied magnetic field, u_0 the average velocity, and ρ, ν, and σ, stand for the thermophysical properties of the fluid, its density, kinematic viscosity, and electric conductivity. Here, Ha is a dimensionless measure for the strength of the magnetic field, Re for velocity and c quantifies the conductance of the wall compared to that of the fluid. Electrically conducting walls are characterized by their electric conductivity σ_w and wall thickness t_w.

The flow is described by the balance of momentum and conservation of mass

$$Re\left(\frac{\partial \mathbf{u}}{\partial t} + (\mathbf{u}\cdot\nabla)\mathbf{u}\right) = -\nabla p + \nabla^2\mathbf{u} + Ha^2\,\mathbf{j}\times\mathbf{B}, \tag{1}$$

$$\nabla\cdot\mathbf{u} = 0, \tag{2}$$

by Ohm's law and an equation for electric potential

$$\mathbf{j} = -\nabla\phi + \mathbf{u}\times\mathbf{B}, \tag{3}$$

$$\nabla^2\phi = \nabla\cdot(\mathbf{u}\times\mathbf{B}). \tag{4}$$

The latter ensures conservation of charge, $\nabla\cdot\mathbf{j}=0$. Here $\mathbf{B}=\hat{\mathbf{y}}$, $\mathbf{u}$, $\mathbf{j}$, p, and ϕ stand for the magnetic field, velocity, current density, pressure and electric potential, scaled by B, u_0, $\sigma u_0 B$, $\rho\nu u_0/L$ and $u_0 BL$, respectively. The magnetic field is assumed constant and not modified by the flow (low R_m limit).

For conducting walls, equations (3) have to be solved also inside the wall with conditions at the fluid wall interface, $\mathbf{u} = 0$, $\phi = \phi_w$, $\mathbf{j}\cdot\mathbf{n} = \mathbf{j}_w\cdot\mathbf{n}$. The external surface of the wall is insulating $\mathbf{j}_w\cdot\mathbf{n}=0$. For thin walls, the potential equation for the wall may be reduced to the so-called thin-wall condition that applies at the fluid-wall interface

$$\mathbf{j}\cdot\mathbf{n} = \nabla_w\cdot\left(c\nabla_w\phi_w\right), \tag{5}$$

where $\mathbf{n}$ denotes the inward unit normal and ∇_w stands for the projection of the gradient operator on the interface.

The geometry and coordinates used to describe Hunt flow in the present paper, are shown in Figure 1. Here x denotes the streamwise coordinate, the magnetic field is parallel to the non-conducting side walls and aligned with y. In the sketch all dimensions are scaled with the Hartmann length, i.e. the duct has nondimensional extensions $-1\le y\le 1$ and $-d\le z\le d$, where d stands for the aspect ratio. Electric potential data on the fluid-wall interface is discussed below along a circumferential coordinate s as shown in the sketch.

For strong magnetic fields ($Ha\gg 1$) the flow exhibits a core with essentially uniform velocity and thin Hartmann layers of thickness $\delta_H\sim Ha^{-1}$ in which the velocity drops to zero at the Hartmann walls. Side layers have a thickness $\delta_s\sim Ha^{-1/2}$ in which the high-velocity jets are located.

The stability of Hunt flow and its transition to time-dependent and eventually fully turbulent conditions has been analyzed for various combinations of Ha and Re, for different aspect ratios d, and for different wall conductivities c. Results have been obtained by experiments performed in the MEKKA laboratory at the Karlsruhe Institute of Technology, by a linear stability analysis and numerical simulations in the weakly nonlinear regime, and by high-resolution direct numerical simulations for states that might approach full turbulence.

3. Experiments

The design of the employed liquid metal loop and details of the test section are shown in Figure 2. Two lateral ducts serve as electromagnetic conduction pumps that feed the test section in the middle. This double loop configuration aims at realizing the most symmetric velocity distribution at the entrance of the central duct [6]. The entire loop is exposed to a uniform magnetic field (no 3D perturbing effects since the flow is completely inside the magnet), that yields Hartmann numbers up to Ha=2700. With a current of 2000A in both pumps it is possible to reach Reynolds numbers up to $Re\approx 6\cdot 10^4$.

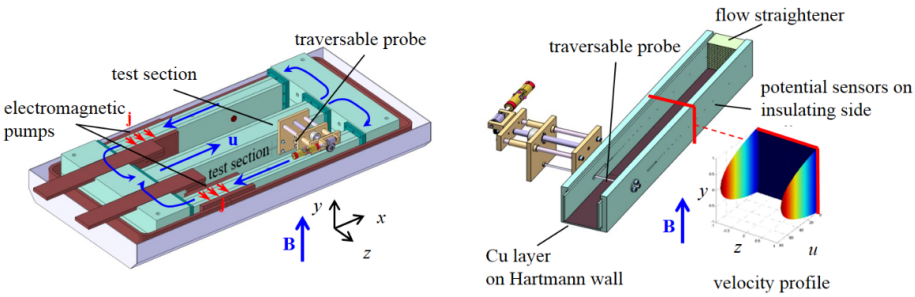

Figure 2. Liquid metal double loop with electromagnetic pumps, central test section, and details of the test section with copper layers on Hartmann walls. The entire loop is placed in a uniform magnetic field.

The test section has two electrically insulating walls parallel to the magnetic field. Electrically conducting Hartmann walls at a distance $2L$=60mm are realized by lamination of non-conducting walls with thin foils of copper (t_w=50μm) yielding c=0.03. Distribution of electric potential along the side-walls and along one Hartmann wall is measured at a number of electrodes. A traversable probe is used to measure profiles of transverse potential gradient within the fluid at y=0 for $-d<z<d$ to estimate the

axial velocity $u(y=0,z)\approx\Delta\phi/\Delta z$ between the tips of the probe over their distance Δz=1.6mm. The distance between flow straightener at the entrance and the instrumented cross-section is about 15L which should be long enough that the flow becomes fully developed far upstream of the instrumented cross-section [7] [6]. GaInSn is used as model fluid so that experiments can be performed at room temperature. Good electrical contact between fluid and conducting Hartmann walls has been achieved by first cleaning the metallic surfaces using hydrochloric acid and by rubbing GaInSn into the copper [8]. This procedure avoids contact resistance between the fluid and the copper surface and yields consistent results [9].

Potential signals consist of a mean part, a fluctuating part and noise, $\Delta\phi=\Delta\overline{\phi}+\Delta\phi'$+noise. The mean potentials on the duct walls are recorded by a Beckhoff KL3312 system and potentials at the tips of the traversable probe by a Prema 8017 nanovolt meter with resolution of 100nV. A multichannel, in-house developed system with an amplification factor of 5000 has been used to investigate time-dependent signals of potential differences of the order of 10^{-6} V. After a moderate pre-amplification an analog high-pass filter removes the mean part $\Delta\overline{\phi}$ with a cut-off frequency of 2Hz, then the time-dependent signals are strongly amplified, and a digital low-pass filter with a cut-off frequency of 95Hz is applied to remove high-frequency noise.

Instability of Hunt-type flow was investigated experimentally first for square ducts with aspect ratio d=1 for Hartmann numbers $500 \le Ha \le 2000$ and Reynolds numbers $Re\lesssim$30000. One example of potential and velocity data is shown in Figure 3. We observe a linear variation of ϕ along the Hartmann wall and parabolic-like behaviour along the side walls. The agreement of measured wall potential data (symbols) with results of an exact analytical solution [10] is perfect for small Re. For higher Re, data of potential at the side walls shows slightly smaller magnitude which is a clear indication that the flow rates carried by the jects become smaller as a result of unsteady or eventually turbulent flow in the side layers. This is confirmed by measurements of potential gradients at the movable probe as indication of velocity $u(y=0,z)\approx\Delta\phi/\Delta z$. Results shown in Figure 3 agree again well with the laminar analytical predictions for moderate Re. Instabilities at Re=15637 lead to an increased momentum transfer, reduction of maximum velocity in the jets and thickening of the layers.

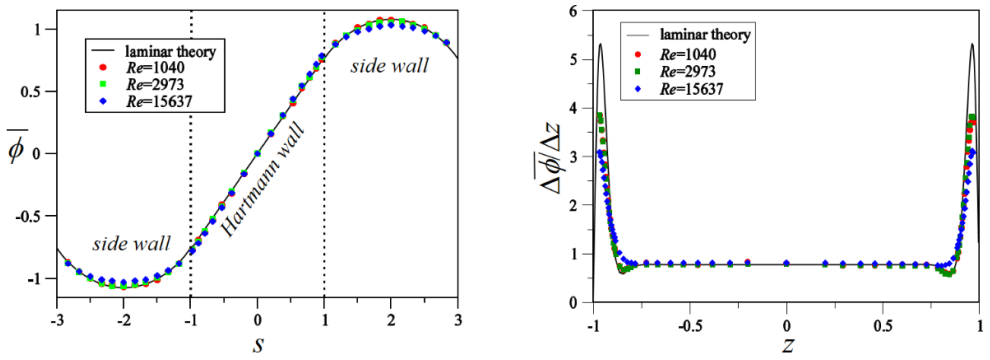

Figure 3. Mean potential distributions along the wall of a square duct and velocity profiles $\overline{u}(y=0,z)\approx\Delta\overline{\phi}/\Delta z$ for Ha=1000.

A systematic investigation for the onset of instabilities was performed in the following way: for a given strength of the magnetic field, i.e. for fixed Ha, the flow rate in terms of Re was increased while potential signals obtained at the probe and from walls were recorded. The onset of unstable flow i.e. the critical Reynolds number Re_c was obtained when measured potential fluctuations clearly emerge from the electromagnetic noise of the measuring circuit.

Values of critical Reynolds numbers obtained by this method are shown in Figure 4. We observe first an apparently *stable laminar* regime when $Re<Re_{c,I}$. Above $Re_{c,I}$ the flow is time-dependent and perturbations have measurable amplitude. These instabilities are located close to the side walls while

the core of the flow is practically still not affected by the instability. This flow regime is indicated in the figure as *unstable regime I*. Increasing *Re* further, leads to the sudden occurrence of perturbations with amplitudes that are one or two orders of magnitude larger. This transition into another *unstable regime II* is also indicated in the diagram. In *unstable regime II* the core flow is also affected and perturbations become visible on the Hartmann walls. The *unstable regime 0* was detected only for higher *Ha*. Here, instabilities occur at much smaller values of *Re*. By increasing *Re* in this regime the flow becomes apparently laminar again before a transition to *unstable regime I* occurs.

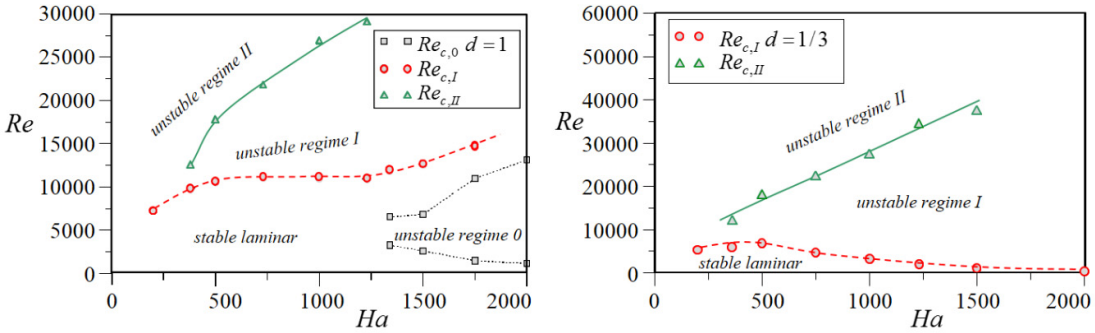

Figure 4. Map of flow regimes as a function of *Ha* for a square duct *d*=1 and for aspect ratio *d*=1/3.

Time-dependent potential gradient data has been recorded simultaneously along a line on a side wall. Two particular results are shown as an example in Figure 5. The coordinate *t* stands for time, scaled by L/u_0. Alternatively, assuming Taylor's hypothesis, we may interpret *t* as axial coordinate *x*=-*ct*, where *c* stands for the velocity at which perturbations move downstream. For *Re*=17506 we observe small-scale structures. Transition to large-scale patterns and higher modes along *y* are observed at *Re*=26599.

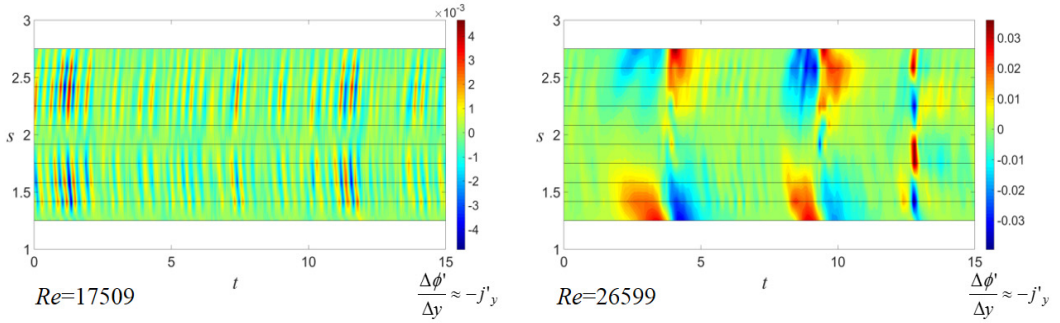

Figure 5. Data of $\Delta\phi'/\Delta y(y,t)$ along the side wall at *z*=1 for *Ha*=1000, showing small-scale structures for *Re*=17506 and transition to large-scale patterns and higher modes along *s* (i.e. along *y*) at *Re*=26599 and aspect ratio *d*=1.

In a second series of experiments, the aspect ratio of the duct was changed to $d = 1/3$ and measurements were performed for Hartmann numbers $500 \leq Ha \leq 2000$ and Reynolds numbers $500 \lesssim Re \lesssim 37000$. Time averaged results for the velocity distribution in transverse direction are presented in Figure 6 for two values of *Ha* and various *Re*. For the smallest *Re*, good agreement between measurements and laminar theory can be observed. With increasing *Re* the maximum jet velocity decreases and the jets become thicker which indicates unstable flow. This decrease of velocity occurs for *Ha*=500 in both jets, causing a symmetric velocity profile. For *Ha*=2000 the velocity profile is non-symmetric for $Re \geq 5054$. As a result the jet at $z = 0.3$ becomes unstable much earlier, while the other one at $z = -0.3$ does not show any thickening until $Re = 25782$. A map of flow regimes for *d*=1/3 showing transitions between *stable laminar* flow, unstable flow with very small fluctuations (*unstable regime I*), and unstable flow with large amplitude (*unstable regime II*) is displayed in Figure 4. Further

results and more details can be found in [11], [12]. Finally it is worth to notice that even when the flow is strongly time-dependent, the pressure drop measured in the experiment still follows the laminar predictions [12].

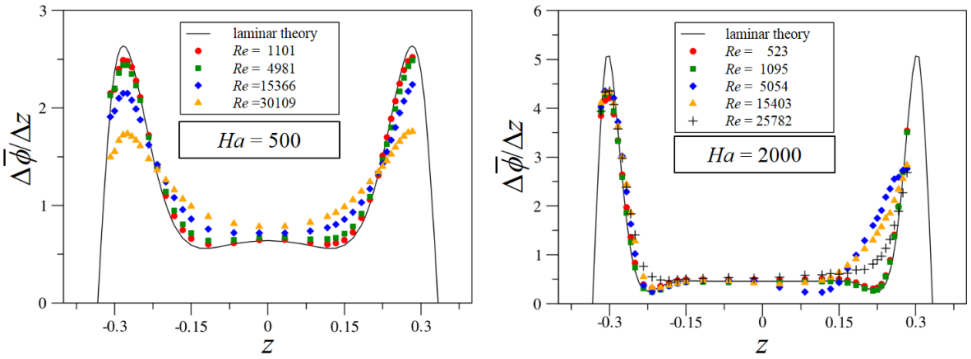

Figure 6. Mean velocity profiles $\bar{u}(y=0,z)\approx\Delta\bar{\phi}/\Delta z$ for Hunt flow with aspect ratio d=1/3.

4. Stability analysis and weakly nonlinear numerical simulations

A linear stability analysis was performed to determine theoretically the critical Reynolds number for the onset of instabilities. Direct numerical simulations were conducted for confirmation of the analysis and for further investigation of the nonlinear unstable flow behaviour in a certain range above the stability limit.

For the linear stability analysis pressure is eliminated by taking the curl of (1), the vorticity $\boldsymbol{\omega}=\nabla\times\mathbf{v}$ is introduced, and the velocity is defined through a vector potential $\boldsymbol{\psi}$ as $\mathbf{v}=\nabla\times\boldsymbol{\psi}$ that satisfies identically mass conservation (2). The equations are linearized assuming a fully developed steady state with infinitesimally small perturbations of all variables that are assumed to have an axial wave number k.

$$(\boldsymbol{\omega},\boldsymbol{\psi},\phi)(x,y,z,t)=(\bar{\boldsymbol{\omega}},\bar{\boldsymbol{\psi}},\bar{\phi})(y,z)+(\hat{\boldsymbol{\omega}},\hat{\boldsymbol{\psi}},\hat{\phi})(y,z)\exp(ik(x-st)). \tag{6}$$

The real part of the complex variable s denotes the phase velocity and the imaginary part vanishes at marginal stability. The resulting eigenvalue problem is obtained by discretization with a Chebychev collocation method and solved using the Fortran LAPACK package. For efficient performance of the solution method, the problem is considered only in a quarter of the duct assuming appropriate symmetry conditions as shown in Table 1. A detailed formulation of the problem and results can be found in [13], [14] and [15].

mode	y-symmetry	z-symmetry
I	even	even
II	odd	even
III	even	odd
IV	odd	odd

Table 1: Symmetries of vorticity perturbations in magnetic field direction [13]

The results presented in the following have been obtained for Hunt flow in ducts with Hartmann walls of arbitrary conductivity c. Figure 7 shows the critical Reynolds number Re_c as a function of Ha for the least stable modes for several values of c. Increasing the magnetic field for well conducting walls (c=1) has first a destabilizing effect at small values of Ha. After passing a local minimum (e.g. $Re_c\approx 1700$ at $Ha\approx 11$ for $c=1$), Re_c increases until mode I becomes the most unstable one (e.g. at $Ha\approx 46$ for $c=1$). This mode shows strong decrease of Re_c with increasing Ha. If $cHa\gg 1$, Re_c shows only weak dependence on Ha. A similar behavior has been reported from previous studies [2] [13]. The dependence

of the critical wavenumber k_c on Ha is shown in Figure 7. At small Ha, k_c shows only moderate variation with Ha. But for higher Hartmann numbers, when mode I becomes most unstable, the critical wavenumber k_c increases as $k_c \sim Ha^{1/2}$ for $Ha \to \infty$. This shows that the wave length $\lambda_c = 2\pi/k_c \sim Ha^{-1/2} \sim \delta_s$ becomes proportional to the thickness of the side layers, which is a clear indication that the instability is triggered by the physics in the side layers.

Analyses for different aspect ratios have been also performed. A presentation of all results is out of scope of the present paper. Further details can be found in [14]

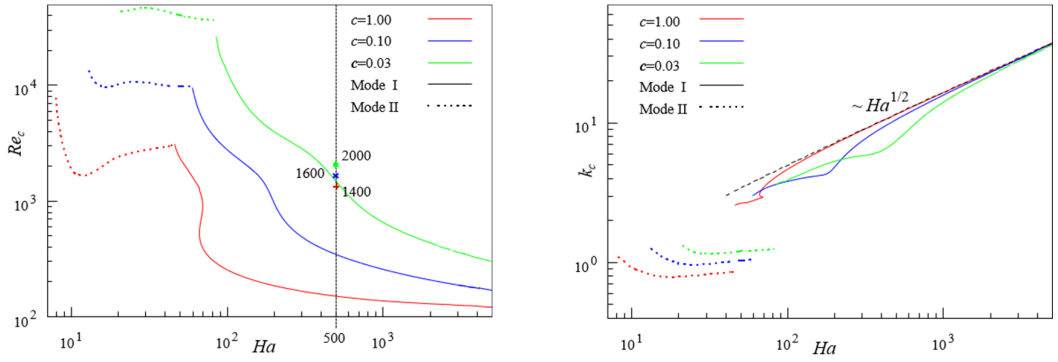

Figure 7. Hunt flow in a square duct. Critical Reynolds number Re_c and wave number k_c as a function of Ha for different wall conductance ratios c. Symbols at Ha=500 in left figure denote parameters used later in numerical simulations.

Results obtained by the linear stability analysis have been verified with numerical simulations for parameters close to the critical Reynolds number $Re_c(Ha)$ using OpenFoam [16]. A wall conductance ratio c=0.03, as present in the experiment, was chosen. For Ha=500 the linear stability analysis yields $Re_c \approx 1490$. A number of numerical simulations were performed for $Re<Re_c$ and for $Re>Re_c$ as indicated by symbols in Figure 7. For Re=1400$<Re_c$ the flow is stable and stationary with no variations of variables along the streamwise direction. This can be seen from Figure 9 in which the axial component of velocity near the side wall at y=0, z=0.96 is displayed. The agreement with the exact analytical solution is very good and deviations are smaller than 0.3%. When the Reynolds number is increased to Re=1600$>Re_c$ one can observe small wavy perturbations (Figure 9), which confirms that the flow is already unstable. However, the magnitude of perturbations is still very small and the maximum value of turbulent kinetic energy is $E_{kin} = \overline{u'^2} = O\left(10^{-6}\right)$. Patterns of axial velocity perturbations u' at Ha=500 obtained at the stability threshold by the linear theory and at slightly supercritical Re by OpenFOAM are quite similar as displayed in Figure 8.

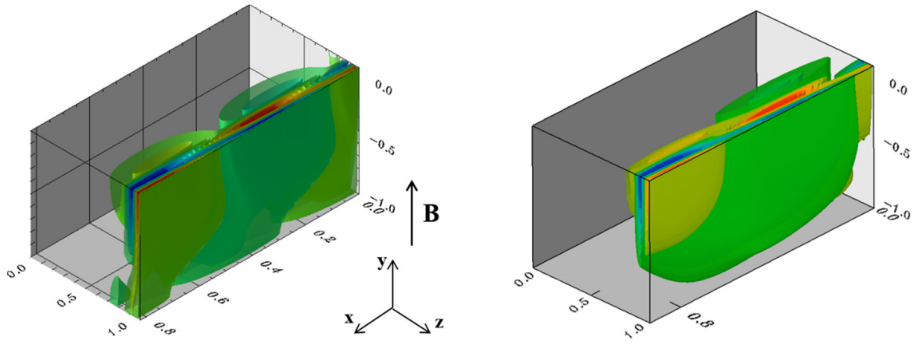

Figure 8. Hunt flow at Ha=500. Perturbations of velocity u' determined by the linear stability analysis at $Re_c \approx 1500$ (left) and OpenFOAM (right) at Re=1600. Only a quarter of the duct is shown.

When the Reynolds number is further increased up to Re=2000 the magnitude of perturbations becomes much stronger (Figure 9), and E_{kin} reaches values up to $E_{kin}=O(10^{-1})$. Finally we may conclude that both, the linear stability analysis and the numerical simulations, predict the onset of time-dependent motion at nearly the same critical Reynolds number. In the experiment, however, first occurrence of instabilities at Ha=500 could be detected only for $Re>10^4$. This apparent disagreement might be explained by the fact that the used experimental hardware has difficulties to detect small perturbations with frequencies below 2Hz while the numerical predictions and the stability analysis yield values close to 1.4Hz at the onset of instability.

Perturbations of potential gradients $\partial_y\phi'$ are visualized on the side wall in Figure 10 for Ha=500 and Re=2000. Results obtained in experiments show qualitative agreement (Figure 5) [12].

The present paper can give only a brief overview about the stability analysis and weakly nonlinear numerical simulations. Further results and details can be found e.g. in [14], [15], [17].

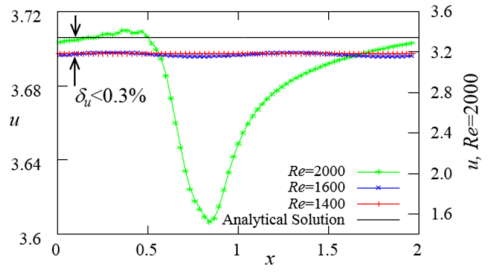

Figure 9. Numerical results for streamwise velocity $u(x,z=0.96)$ for different Re at Ha=500. Note: The axis for Re=2000 is shown at the right side.

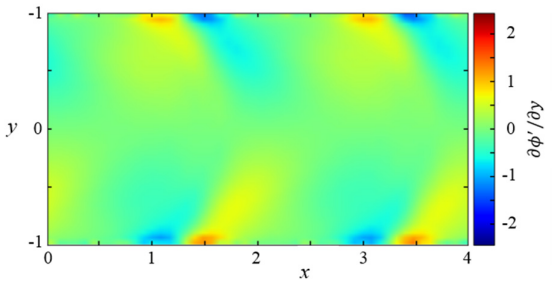

Figure 10. Numerical results for $\partial_y\phi'$ at the side wall for Re=2000 at Ha=500.

5. High-resolution direct numerical simulations

The linear stability analyses and numerical simulations with OpenFOAM focused on the onset of instabilities and the behavior at fairly low Reynolds numbers. Direct numerical simulations (DNS) at high Reynolds numbers approaching those realized in experiments have been performed with a finite-difference code for the rectangular duct geometry [18]. The computational grid is based on non-equidistant grid spacing which can be clustered near walls by one-dimensional mappings for the y- and z-directions. Thanks to this structured grid layout, the code is parallelized by one-dimensional domain decomposition, and the Poisson equations for pressure and electric potential are solved very efficiently by fast Fourier transforms and the two-dimensional cyclic reduction method implemented in the FISHPACK library [19]. For this reason, numerical resolutions of up to 2048×384×384 grid points could be realized.

DNS were performed for the ideal Hunt flow with perfectly conduction Hartmann walls and insulating side walls. The computational domain is assumed periodic in the streamwise direction. Relatively low values of the Hartmann number are considered first, and the changes of the flow with the Reynolds number Re are explored. This is done by systematically increasing or decreasing Re between successive simulations.

For the moderate magnetic fields, i.e. for Ha=100, uniformly spaced columnar vortices appear at the side walls as Re is increased to 500 from the laminar state (see [20]). For Re=1000 these vortices become larger and their spacing wider. When Re is increased further to 1400, large vortical structures appear in localized patches with leading and trailing vortices of smaller size. In all these cases, the flow appears symmetric with respect to the horizontal mid-plane. Concerning the left-right symmetry, the vortices form a staggered pattern, which maintains a constant phase shift. For slightly higher Re of about 1600

the regular vortical structures are replaced by so-called jet detachments, where the jets are lifted away from the wall into the core region. By that, strong perturbations are generated which also affect the opposing side layers and lead to similar detachments there. The detachments are associated with a significant mean turbulent kinetic energy (TKE) of up to 10% of the energy of the mean flow. By contrast, the columnar vortices attached to the side walls at lower *Re* are generally quite weak with a mean TKE below 0.1%. When the Reynolds number is increased further, the mean TKE decreases slowly, and the jet detachments become less pronounced. At the highest *Re*=10000 considered for *Ha*=100, the side wall regions exhibit turbulent bands with small-scale vortices, and the core region fluctuates less than in the presence of detachments. When the Reynolds number is systematically decreased from such a high value, the jet detachments reappear and increase in strength down to *Re*=2000. However, detachments do not disappear when *Re* is further reduced. Instead, they persist down to *Re*=200 although the mean TKE is gradually decreasing. This hysteresis indicates a complex behavior with a multiplicity of different states. In this respect, the behavior resembles subcritical transition in certain other shear flows although the linear stability is presumably supercritical in the present case.

Flows at higher Hartmann numbers up to *Ha*=1000 have been also explored for increasing *Re*. Different states are shown in Figure 11 as instantaneous velocity snapshots, visualized in the horizontal plane *y*=0. Unevenly spaced groups of weak detachments appear already at *Re*=1000. With increasing *Re*, there is a progression to detachments that spread into the core. At *Re*=10000 the level of turbulence in the core region is strongest. It diminishes with increasing *Re*, and at *Re*=50000 there are turbulent bands at the side layers and the core is weakly fluctuating. This change of flow regimes is also illustrated in Figure 12 for *Re*=1000 – 50000 by instantaneous distributions of streamwise velocity. We observe that the strongest flow distortions occur at *Re*=10000.

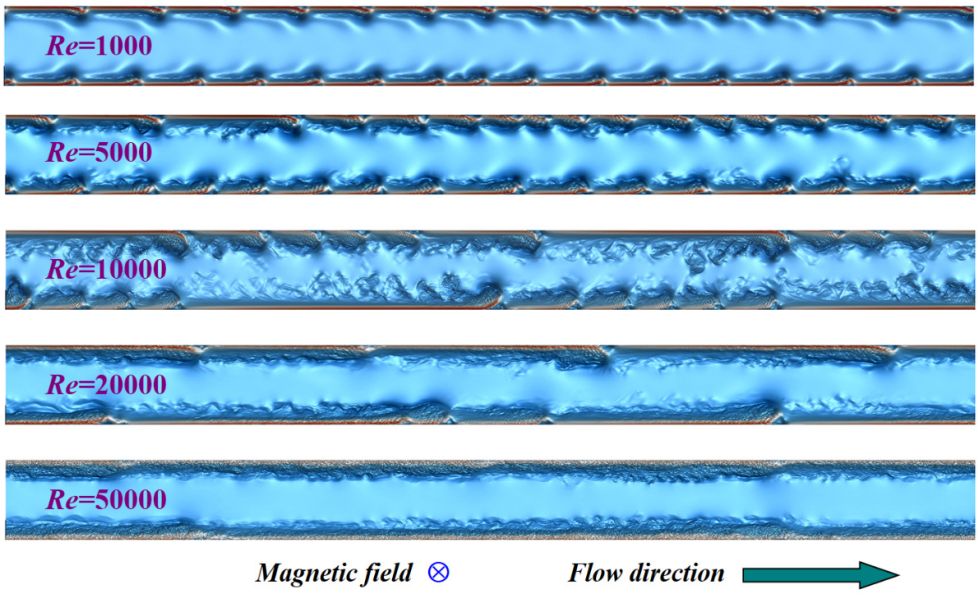

Figure 11. Hunt flow in a square duct at *Ha*=1000 and *Re*=1000 – 50000. Instantaneous patterns of streamwise velocity are visualized in the mid-plane at *y*=0.

Near *Re*=1000 also multiple states have been observed [19]. Especially for this study a series of simulations has been conducted at *Ha*=1000 with decreasing *Re*, similar to [20]. Several target values in the range 500>*Re*>100 were checked. In all cases the flow at *Re*=1000 with jet detachments (Figure 11) was used as initial state. These simulations reveal the interesting observation that no weak structures, such as small-scale vortices [2], have been obtained. Instead, the flow domain remains populated with

detached jets of gradually decreasing TKE while decreasing *Re*. The observed behavior of hysteresis corresponds again to approximately the same range *Re* = 200...1000 and at *Re*=100 the flow becomes fully laminar as in the low-*Ha* case. The latter observation perfectly confirms the results of a linear stability analysis of Hunt flow, where the critical Reynolds number Re_c=112 has been predicted for *Ha*≫1 [13].

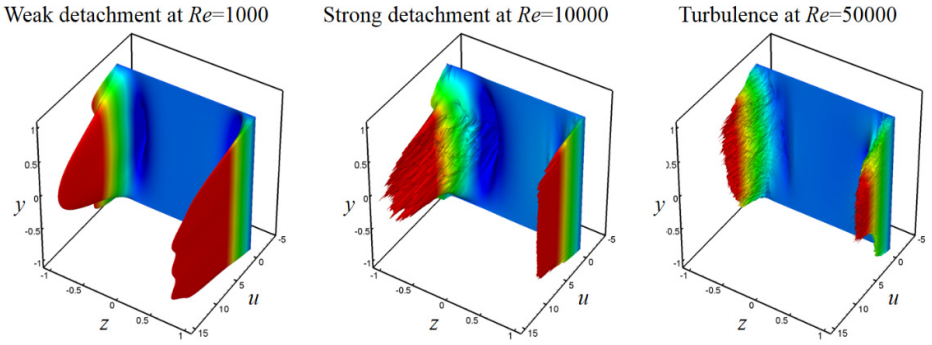

Figure 12. Instantaneous velocity profiles of Hunt flow in a square duct for *Ha*=1000.

Usually magnetic fields are known to suppress turbulent or time-dependent motion. However, in the present case of Hunt flow, the magnetically induced jets are a source of instability. In order to judge the stabilising and destabilizing mechanisms caused by the Lorentz force, reduced settings are postulated: the flow is driven by the balance between pressure gradient and streamwise constant Lorentz force obtained by axial averaging of turbulent Hunt flow. This force which is applied as source term in the momentum equation for hydrodynamic simulations is able to produce the Hunt jets that become unstable and turbulent. As can be seen in Figure 13 and Figure 14, the side layers then show very strong turbulent fluctuations down to the lowest Reynolds numbers. Figure 14 also highlights that the core region is far more turbulent and that the velocity in the side layers is reduced. The reason for this behavior lies in the fact that the strong correlation of fluctuations along magnetic field lines and associated Joule damping is absent in this hypothetical flow. Moreover, we observe that the time-dependent flow regimes cease only at extremely low *Re*≈10. We thereby confirm that the magnetic damping effect on individual eddies is essential for the observed transitional flow states.

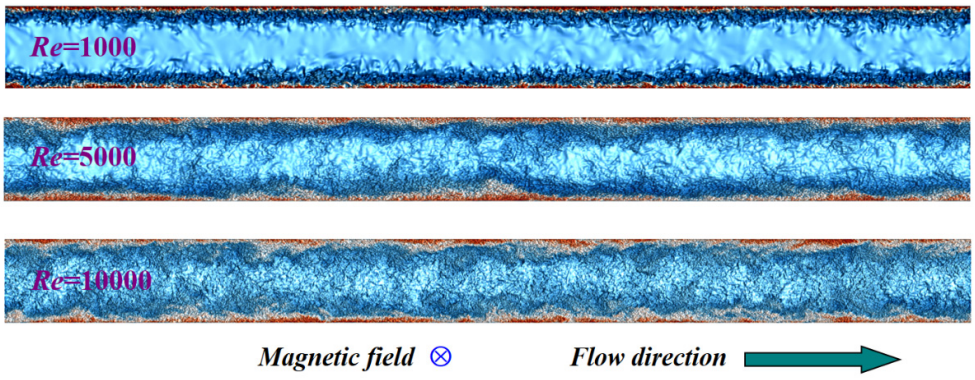

Figure 13. Numerical simulations of Hunt flow in a square duct at *Ha*=1000 and *Re*=1000 – 10000 with Lorentz force computed from the streamwise-averaged flow. Instantaneous patterns of streamwise velocity are visualized in the mid-plane at *y*=0.

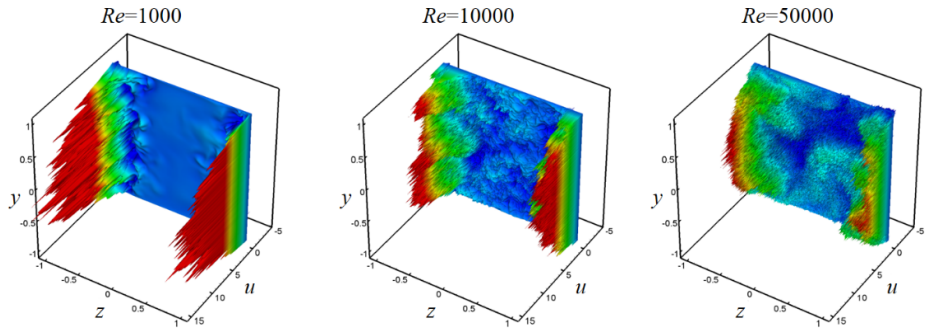

Figure 14. Instantaneous velocity profiles of Hunt flow in a square duct at *Ha*=1000 when the Lorentz force density is computed from the streamwise-averaged flow.

Direct numerical simulations have shown that transition in Hunt flow proceeds through different stages and some of them may be difficult to detect in experiments on account of the very small amplitude of fluctuations and the occurrence of multiple states. A direct comparison between simulations and experiments is also problematic due to the use of periodic boundary conditions for the computations. Spatial simulations with details of a flow straightener as inlet condition may seem more appropriate but they are computationally very expensive when *Ha* and *Re* are large

6. Conclusions

Magnetically induced instabilities in liquid metal duct flows have been studied for Hunt flow by a linear stability analysis, numerical simulations close to the onset of time-dependent motion, and by direct numerical simulations for high Reynolds numbers. The onset of time-dependent flow patterns and their intensity depends on the strength of the magnetic field and on the flow rate in terms of the Hartmann number *Ha* and Reynolds number *Re*. Numerical simulations show that unstable structures close to the stability limit have very small amplitude and occur in a fairly low frequency range that makes their experimental detection under laboratory conditions extremely challenging. This fact may explain difficulties in past and present comparisons of theoretical results and experimental observations. High-resolution direct numerical simulations give detailed insight into the rich variety of completely different flow patterns that might even coexist for the same set of parameters.

Acknowledgement

Financial support of this research by the German Helmholtz Association in the frame of the Helmholtz-Alliance LIMTECH is gratefully acknowledged. Computer resources were provided by the computing centers of Coventry University, Forschungszentrum Jülich (NIC) and TU Ilmenau.

References

[1] Smolentsev S, Badia S, Bhattacharyay R, Bühler L, Chen L, Huang Q, Jin H-G, Krasnov D, Lee D-W, Mas de les Valls E, Mistrangelo C, Munipalli R, Ni M-J, Pashkevich D, Patel A, Pulugundla G, Satyamurthy P, Snegirev A, Sviridov V, Swain P, Zhou T and Zikanov O 2015 *Fusion Engineering and Design* **100** 65-72

[2] Ting A L, Walker J S, Moon T J, Reed C B and Picologlou B F 1991 *Int. J. Engng. Sci.* **29** 939-948

[3] Reed C B and Picologlou B F 1989 *Fusion Technology* **15** 705-715

[4] Burr U, Barleon L, Müller U and Tsinober A B 2000 *Journal of Fluid Mechanics* **406** 247-279,

[5] Hunt J C R 1965 *Journal of Fluid Mechanics* **21** 577-590

[6] Bühler L, Mistrangelo C und Koehly C 2012 *IEEE Transactions on Plasma Science* **40** 590-595
[7] Gelfgat Y M, Dorofeev V S and Shcherbinin E V 1973 *Magnetohydrodynamics* **7** 26-29
[8] Morley N B, Burris J, Cadwallader L C and Nornberg M D 2008 *Review of Scientific Instruments* **79** 056107
[9] Chowdhury V, Bühler L and Mistrangelo C 2014 *Fusion Engineering and Design* **89** 1299-1303
[10] Müller U and Bühler L 2001 *Magnetofluiddynamics in Channels and Containers* (Wien, New York: Springer)
[11] Chowdhury V, Bühler L and Mistrangelo C 2016, in *Proceedings of the 10th PAMIR Int. Conference Fundamental and Applied MHD, Cagliari - Italy, June 20 - 24*, pp. 145-149
[12] Chowdhury V, PhD Thesis, Karlsruhe Institute of Technology, 2016
[13] Priede J, Aleksandrova S and Molokov S 2010 *Journal of Fluid Mechanics* **649** 115-134
[14] Arlt T, Priede J and Bühler L 2017 *Magnetohydrodynamics* **53** 35-44
[15] Priede J, Arlt T and Bühler L 2016 *Journal of Fluid Mechanics* **788** 120-146
[16] Mistrangelo C and Bühler L 2011 *Fusion Science and Technology* **60** 798-803
[17] Arlt T, Priede J and Bühler L 2017 *Journal of Fluid Mechanics,* in press
[18] Krasnov D, Zikanov O and Boeck T 2011 *Computers and Fluids* **50** 46-59
[19] Krasnov D, Boeck T, Braiden L, Molokov S and Bühler L 2016 Karlsruhe Institute of Technology, KIT-SR 7713, ISBN 978-3-7315-0562-4
[20] Braiden L, Krasnov D, Molokov S, Boeck T and Bühler L 2016 *Europhysics Letters* **115** 44002